MITSUBISHI ELECTRIC RESEARCH LABORATORIES
http://www.merl.com

Bean's Critical-State Model as a Consequence of the Circuit Model of Non-linear Resistance

Lin, C.

TR2019-031 June 22, 2019

Abstract

Bean's critical-state model has been the foundation to compute the heat generated by the time-varying magnetic field or current in type-II superconductors. Two key features of the Bean model are (i) the current density is either zero or at the critical value Jc, and (ii) the change of current distribution begins at the surface. In this work, we apply the circuit model to simulate the process of charging a type-II superconductor. In addition to the self and mutual inductances among the basic units, we introduce a current-dependent longitudinal resistance to describe the critical current density, above which the conductor becomes resistive. By identifying the inductance values, we are able to reproduce the characteristic behavior of the Bean model. Specifically we consider a superconducting slab, a superconducting wire composed of straight or twisted filaments, and recover the established analytical results for these geometries. In terms of the circuit model, the behavior of the Bean model is a consequence of the geometry-specific structure of inductances and the non-linear resistances. Besides offering an intuitive explanation of the Bean model, our circuit-model calculations provide concrete examples to show that it can be used to simulate the complete charging process of multi-filament superconducting wires.

Journal of Applied Physics

Bean's Critical-State Model as a Consequence of the Circuit Model of Non-linear Resistance

Chungwei Lin[1]
Mitsubishi Electric Research Laboratories, 201 Broadway, Cambridge, MA 02139, USA

(Dated: 11 February 2019)

Bean's critical-state model has been the foundation to compute the heat generated by the time-varying magnetic field or current in type-II superconductors. Two key features of the Bean model are (i) the current density is either zero or at the critical value J_c, and (ii) the change of current distribution begins at the surface. In this work, we apply the circuit model to simulate the process of charging a type-II superconductor. In addition to the self and mutual inductances among the basic units, we introduce a current-dependent longitudinal resistance to describe the critical current density, above which the conductor becomes resistive. By identifying the inductance values, we are able to reproduce the characteristic behavior of the Bean model. Specifically we consider a superconducting slab, a superconducting wire composed of straight or twisted filaments, and recover the established analytical results for these geometries. In terms of the circuit model, the behavior of the Bean model is a consequence of the geometry-specific structure of inductances and the non-linear resistances. Besides offering an intuitive explanation of the Bean model, our circuit-model calculations provide concrete examples to show that it can be used to simulate the complete charging process of multi-filament superconducting wires.

I. INTRODUCTION

Superconducting (SC) magnets, which use the type-II superconductors[1,2] to carry the SC current, are compact equipment that can generate a large magnetic field[3,4]. Its application ranges from confining the near speed-of-light charged particles in particle accelerators[5,6] to generating a large and stable magnetic field for Magnetic Resonance Imaging[7] and Nuclear Magnetic Resonance[8]. According to Bean's critical-state model [9], the current density inside a type-II superconductor is either at its critical value J_c or zero; this implies that any small temperature or flux perturbations are dangerous as these perturbations make the critical-state regions locally resistive, and the resulting Joule heating can potentially quench the whole SC magnets[10]. The other characteristic of the Bean model is that the change of the SC current begins at the surface and then gradually propagates into the superconductor. This feature naturally leads to the hysteresis phenomena and is verified by the magnetization measurements[11,12]. Since then, the Bean model has been served as the starting point to compute the heat generation caused by the changing field or current, based on which the quench criterion is established.[3,4,13–18].

The circuit model, either the distributed parameter version [19,20] or the lumped parameter version[21–23], has been developed to compute the current distributions among SC filaments or wires[24,25], and to study the subtle responses of SC wires/filaments to the changes of the external magnetic field [19–21]. Currently, the use of circuit model mainly focuses on the regime where the SC current is much smaller than its critical value, where the resistance is practically zero. In this work, we demonstrate that the circuit model can well describe the phenomena near the critical current by introducing a current-dependent resistance. In particular, we show that the circuit model, when taking the proper limit, reproduces a few established results obtained using the Bean model. Our calculations not only expand the applicable regime of the circuit model, but also provide an intuitive explanation of the origin of the Bean model.

The rest of this paper is organized as follows. In Section II we briefly review the circuit model established in Ref.[19,20]. We will introduce the non-linear resistance to the dynamical equations and point out the subtleties of solving them. In Section III we apply the circuit model for charging a semi-infinite SC slab. In Section IV we apply the circuit model for charging a SC wire composed of straight SC filaments. The relation between the Bean model and the circuit model is discussed. In Section V we apply the circuit model for charging a SC wire composed of twisted SC filaments. For SC geometries considered in Sections III, IV, V, the established analytical expressions are provided and discussed within the framework of the circuit model. A brief conclusion is given in Section VI.

II. DISTRIBUTED PARAMETER CIRCUIT MODEL

We recapitulate the dynamical equations (a set of partial differential equations, PDE) based on the distributed parameter circuit model [19,20]. A few subtle points of solving these equations are pointed out. As we will solve the dynamical equations by discretizing the real space (instead of the basis function expansion [19,20]), the difference between the distributed parameter model and the lumped parameter model[21–23] is a matter of spatial resolution. The non-linear resistance is introduced and the heat caused by the current injection is computed.

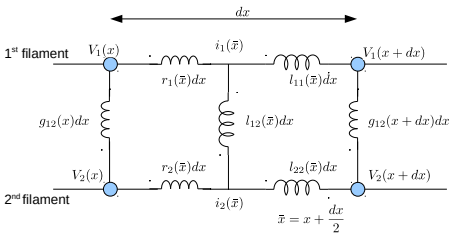

FIG. 1. The distributed parameter circuit model composed of two filaments. The external voltage sources are neglected. $V_n(x)/i_n(x)$ is the voltage/current of nth filament at position x. In the numerical simulation, the mesh points of voltages ($V(x)$) and those of currents ($i(\bar{x})$) are chosen to be alternate in space. $\bar{x} = x + \frac{dx}{2}$ illustrates this mesh choice.

A. The dynamical equations

Following Refs.[19,20], we consider a superconducting wire composed of N filaments which are the building blocks of the circuit model. Over the length dx, the filaments have longitudinal resistances $R_i = r_i dx$ ($i = 1, ..., N$) where r_i are the longitudinal resistances per unit length of filament (zero if the filament is in the SC state). The self inductances of the filaments are denoted as $L_{ii} = l_{ii} dx$ whereas the mutual inductances between filaments $L_{ij} = l_{ij} dx$. The values of the inductance matrix l_{ij} depend on the geometry of interest. It turns out that only differences between these parameters affect the dynamics [Section II B]. This implies that l_{ij} can all be divergent: as far as $l_{ij} - l_{00}$ for all i, j are well defined, the PDE permits a solution. Finally, each filament can have an external voltage source $V_i^{ext} = v_i^{ext} dx$ which we do not consider in this paper. The circuit model with two filaments is represented schematically in Fig. 1.

Using the basic electrodynamics, the dynamical equations can be cast as

$$\frac{\partial \mathbf{v}}{\partial x} = -\mathbf{r}\mathbf{i} - \mathbf{l}\frac{\partial \mathbf{i}}{\partial t} + \mathbf{v}^{ext}, \tag{1a}$$

$$\frac{\partial \mathbf{i}}{\partial x} = \mathbf{g}\mathbf{v}, \tag{1b}$$

$$\text{with } \sum_{h=1}^{N} i_h(t) = I_{tot}(t), \tag{1c}$$

with $I_{tot}(t)$ the total current carried by the SC wire. In Eqs. (1), we have defined the position-dependent vectors of voltage, current, and external voltage as

$$\mathbf{v} = \begin{bmatrix} V_1 & V_2 & \dots & V_N \end{bmatrix}^T, \tag{2a}$$

$$\mathbf{i} = \begin{bmatrix} i_1 & i_2 & \dots & i_N \end{bmatrix}^T, \tag{2b}$$

$$\mathbf{v}^{ext} = \begin{bmatrix} v_1^{ext} & v_2^{ext} & \dots & v_N^{ext} \end{bmatrix}^T (\equiv 0), \tag{2c}$$

and the position-dependent matrices of longitudinal resistance, inductance, and inter-filament con-

ductance as

$$\mathbf{r} = \mathrm{Diag}\left[r_1 \;\; r_2 \;\; \ldots \;\; r_N\right], \tag{3a}$$

$$\mathbf{l} = \begin{bmatrix} l_{11} & l_{12} & \ldots & l_{1N} \\ l_{21} & l_{22} & \ldots & l_{2N} \\ \vdots & \vdots & \ldots & \vdots \\ l_{N1} & l_{N2} & \ldots & l_{NN} \end{bmatrix}, \tag{3b}$$

$$\mathbf{g} = \begin{bmatrix} -\sum_{k=2,k\neq 1}^{N} g_{1k} & g_{12} & \cdots & g_{1N} \\ g_{21} & -\sum_{k=1,k\neq 2}^{N} g_{2k} & \cdots & g_{2N} \\ \vdots & \vdots & \ldots & \vdots \\ g_{N1} & g_{N2} & \cdots & -\sum_{k=1,k\neq N}^{N} g_{Nk} \end{bmatrix}. \tag{3c}$$

Each component in Eq. (2) represents a basic unit (or a building block) of the circuit model, which is a filament in Fig. 1. If we calculate the spatial derivative of Eq. (1a) assuming that the inter-filament conductances are uniform along the wire axis (i.e., $\partial\mathbf{g}/\partial x = 0$), we obtain the following differential equations for filament currents:

$$\mathbf{gl}\frac{\partial \mathbf{i}}{\partial t} + \frac{\partial^2 \mathbf{i}}{\partial x^2} + \mathbf{gri} - \mathbf{gv}^{ext} = 0, \tag{4}$$

The N equations in Eq. (4) are linearly dependent so the filament currents cannot be uniquely determined until Eq. (1c) is included. We mention that the following equation

$$\mathbf{l}\frac{\partial \mathbf{i}}{\partial t} + \mathbf{g}^{-1}\frac{\partial^2 \mathbf{i}}{\partial x^2} + \mathbf{ri} - \mathbf{v}^{ext} = 0,$$

obtained by taking $\mathbf{g}^{-1}$ on Eq. (4) is not rigorously correct as $\mathbf{g}^{-1}$ does not exist. The correct equation will be presented in Section II B (next subsection).

We wish to emphasize that, although the circuit model is conventionally derived and visualized using filaments as the building blocks, the building block can be more general. In particular, the building block (or the basic unit) of the circuit model can represent SC regions having the same spatial symmetry. Based on this observation, we shall apply the circuit model to describe the SC slab and cylinder (the latter is to model the SC wire).

B. A few remarks on numerics

We now address a few subtleties in solving Eqs. (1). We note that the solution of Eq. (1b) can be loosely expressed as

$$\mathbf{v} = \mathbf{g}^{-1}\frac{d\mathbf{i}}{dx} + v_0(x,t)|e\rangle. \tag{5}$$

with $|e\rangle = [1,1,\ldots,1]^T$. The unknown filament-*independent* voltage function $v_0(x)$ is needed because of $\mathbf{g}|e\rangle = 0$. Eq. (5) is not rigorous because $\mathbf{g}$ has a zero eigenvalue with the eigenvector $|1\rangle \equiv \hat{e} = \frac{1}{\sqrt{N}}(1,1,1...,1)$ ($|1\rangle$ is the normalized $|e\rangle$). In the eigenbasis of $\mathbf{g}$, $\mathbf{g}^{-1}$ is

$$\mathbf{g} = 0|1\rangle\langle 1| + \sum_{i=2}^{N}\lambda_i|i\rangle\langle i| \Rightarrow \mathbf{g}^{-1} = \frac{1}{0}|1\rangle\langle 1| + \sum_{i=2}^{N}\frac{1}{\lambda_i}|i\rangle\langle i|. \tag{6}$$

It is seen that the divergence of $\mathbf{g}^{-1}$ originates from the eigenvector $|1\rangle$. Fortunately, because $I_{tot} = \sum_{k=1}^{N} i_k(x)$ is x-independent, $\frac{\partial \mathbf{i}}{\partial x}$ has no $|1\rangle$ component and only $\mathbf{g}^{-1}$ in the subspace excluding $|1\rangle$ is needed:

$$\mathbf{g}^{-1} \to \tilde{\mathbf{g}}^{-1} = \sum_{i=2}^{N} \frac{1}{\lambda_i} |i\rangle\langle i|. \tag{7}$$

$\tilde{\mathbf{g}}^{-1}$ is computed using $\tilde{\mathbf{g}}^{-1} = [a|1\rangle\langle 1| + \mathbf{g}]^{-1} - a^{-1}|1\rangle\langle 1|$, with a being any non-zero real number. The rigorous form of Eq. (5) becomes

$$\mathbf{v} = \tilde{\mathbf{g}}^{-1} \frac{d\mathbf{i}}{dx} + v_0(x,t)|e\rangle. \tag{8}$$

Substituting Eq. (8) into Eq. (1a) gives

$$\frac{\partial \mathbf{v}}{\partial x} = \frac{\partial}{\partial x}\left[\tilde{\mathbf{g}}^{-1} \frac{d\mathbf{i}}{dx} + v_0(x,t)|e\rangle\right] = -\mathbf{ri} - \mathbf{l}\frac{\partial \mathbf{i}}{\partial t} + \mathbf{v}^{ext}. \tag{9}$$

$v_0(x)$ [or its spatial derivative $\partial v_0(x,t)/\partial x \equiv \alpha(x,t)$] is determined by the requirement of current conservation, i.e., $\frac{d}{dt}\left[\sum_n i_n(x,t)\right] = \frac{d}{dt}\left[\sum_n i_n(x',t)\right]$ for $x \neq x'$. By explicitly including $v_0(x)$ and current conservation, all components of $\mathbf{i}$ are independent variables which significantly facilitates the code implementation. Eq. (9) is as fundamental as Eqs. (1a) and (1b) combined, and will be used to understand the dynamical behavior in subsequent sections. We can use Eq. (9) to prove that adding a constant to the inductance cannot affect the dynamical behavior. If we add a constant c_0 to the inductance matrix, i.e., $\mathbf{l} \to \tilde{\mathbf{l}} = \mathbf{l} + c_0|e\rangle\langle e|$, we find $\tilde{\mathbf{l}}\frac{\partial \mathbf{i}}{\partial t} = \mathbf{l}\frac{\partial \mathbf{i}}{\partial t} + c_0\frac{di_{tot}}{dt}|e\rangle$. As the effect of $c_0\frac{di_{tot}}{dt}|e\rangle$ can be included by redefining $\alpha(x,t)$ but $\alpha(x,t)$ is determined by the total current only, we conclude that adding a constant to $\mathbf{l}$ plays no role in the dynamics.

A few numerical details are now stated. First, we choose mesh points of $v(x)$ and $j(x)$ to be alternate in space to improve the numerical stability[26,27]. Second, the boundary conditions can be specified by (i) the voltages at both ends of each filament, (ii) the current at both ends of each filament with a consistent total current, and (iii) the total current only. We have tested all three types of boundary conditions, but only results of type (iii) will be shown. Finally, we use Runge-Kutta method of order 5 provided in Python Package to implement the time evolution, and have confirmed the numerical accuracy by comparing the results with the analytical expressions provided in Ref.[19].

C. Critical current and non-linear resistance

The critical current density of a superconductor can be described by introducing a current-dependent longitudinal resistance

$$r(i) = r_0 \left(\frac{i}{i_c}\right)^n. \tag{10}$$

This resistance depends on two parameters: the critical current i_c and the "index number" n whose values have to be determined experimentally[4]. The critical current i_c is a function of temperature, magnetic field, and SC geometry; the typical value of n is about 30-40 for a "high-quality" superconductor[4]. When n is large, the resistance $r(i)$ is practically zero when $i < i_c$, but becomes non-negligible when i is close to i_c. When $i \sim i_c$ for a particular filament, the injected current is expected to flow through other filaments of zero resistance until the resistance of that particular

filament becomes zero. With Eq. (10), the circuit model can simulate the entire charging process. For numerical stability, in our simulation we modify Eq. (10) to

$$r(i) = \begin{cases} 0 & \text{if } i \le i_c \\ r_0 \left(\frac{i}{i_c}\right)^n & \text{if } i > i_c \end{cases}. \tag{11}$$

Eq. (11) provides a sharp critical current i_c below which the resistance is strictly zero. Eq. (11) is a good approximation of Eq. (10) when the index number is large, which is usually the case for the low-temperature SC. If the index number is not large, Eq. (10) should be used. It is worth noting that the rapid increase of $r(i)$ near i_c implies that the voltage can vary for a wide range while keeping the filament current around i_c. For this reason, as far as the total current is smaller than $N \times i_c$ (assume all filaments have the same i_c), the current at each filament is bounded by $O(i_c)$. We will show that the non-linear resistance is crucial in reproducing the characteristic behavior of the Bean model. Despite the SC has a very non-intuitive microscopic origin[28–31] and displays complicated vortex structures[32–34] whose motions are responsible for the non-zero resistivity[35–39], the specific form of non-linear resistance Eq. (10) is all we need to capture the essential features of Bean's critical-state model.

D. Heat generation

Within the circuit model, the heat originates from the resistance (Ohm's law) which has longitudinal and transverse components – the former accounts for the heat generated by the intra-filament current whereas the latter inter-filament. The longitudinal part of the dissipation power is given by

$$P_L(t) = \sum_{k=1}^{N} \int dx\, r_k(x) \left[i_k(x,t)\right]^2. \tag{12}$$

If a filament is in the SC state, its longitudinal resistance r_k is zero and therefore $P_L(t) = 0$. If the filament current exceeds the critical value, r_k is non-zero and there will be dissipation. The longitudinal loss is responsible for the self-field effect.

The transverse part of the dissipation power (inter-strand current) is

$$P_T(t) = \frac{1}{2} \sum_{i,j=1}^{N} \int dx\, g_{ij}(x) \left[V_i(x,t) - V_j(x,t)\right]^2. \tag{13}$$

The voltage is computed using $\mathbf{v} = \tilde{\mathbf{g}}^{-1} \frac{\partial \mathbf{i}}{\partial x}$ [see Eq. (7)]. Once obtaining $\mathbf{v}$ (and therefore $V_i(x)$), P_T can be computed using Eq. (13). If the filament current has no spatial dependence, i.e., $i_k(x,t) = i_k(t)$, $\frac{di_k}{dx} = 0$ and $\mathbf{v} = 0$; there is no transverse loss in this case. The transverse loss is usually smaller than the longitudinal loss and we will neglect its contribution.

Determination of the stability condition requires the knowledge of the total heat[40], which can be obtained by integrating the dissipation power over time. As far as the total current is smaller than the maximum SC current $N \times i_c$ which the SC wire can carry, the dissipation power will decay to zero because the current eventually goes through the filaments of minimum (zero) resistances.

III. SUPERCONDUCTING SLAB

In this section we consider the current injection to a SC slab. The main goal is to see how the behavior of Bean's critical-state model is obtained. In particular, we will show that why the

change of SC current starts at the surface and then gradually propagates deeper into the SC slab, and why the SC current is always either at its critical value or zero.

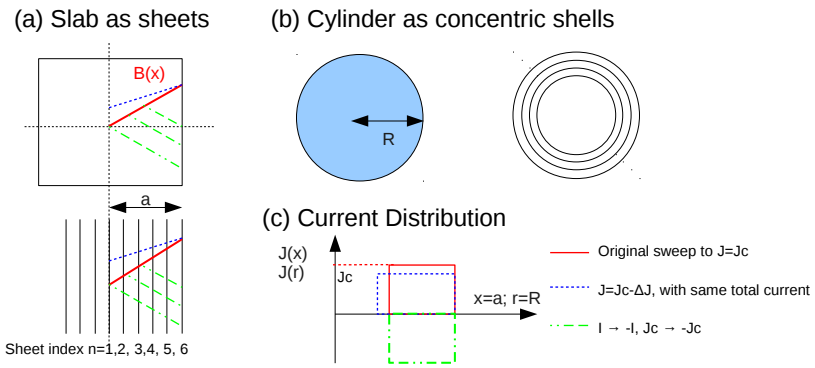

FIG. 2. (a) A SC slab as a collection of sheets, and the magnetic field distribution. (b) A SC cylinder as a collection of concentric shells. (c) The current distribution via minimizing the magnetic energy. In (a), red curve is the "original" magnetic field distribution, with $I_{tot} = J_c a$; the blue dashed curve is the distribution when $J_c \to J_c - \Delta J$, with the same total current; green dash-dot curves represent the change of magnetic field when $I_{tot} \to -I_{tot}$.

A. SC slab as sheets - inductance matrix

A semi-infinite SC slab, with the surface normal defined as $\hat{x}$, is illustrated in Fig. 2(a). The magnetic field can be calculated as

$$B(x) = \mu_0 \int_0^x dx' J(x') = \mu_0 \int_0^a dx' J(x') \Theta(x - x'). \tag{14}$$

In this expression, we implicitly use the boundary condition $B(x = 0) = 0$, i.e., the magnetic field is zero deep inside the SC. We model the SC slab by a collection of sheets, with different sheets corresponding to the different distances to the surface defined at $x = a$. Each sheet serves as a building block of the circuit model.

Next, we determine their self and mutual inductances based on the magnetic energy. The total magnetic energy for $x < a$ is given by

$$\begin{aligned} E_B[J(x)] &= \frac{1}{2\mu_0} \int_0^a dx\, |B(x)|^2 = \frac{\mu_0}{2} \int_0^a dx \left[\int_0^a dx' J(x') \Theta(x - x') \right]^2 \\ &= \frac{\mu_0}{2} \int_0^a dx \int_0^a dx'' J(x') J(x'') \min(a - x', a - x''), \end{aligned} \tag{15}$$

where we have used $\int_0^a dx \Theta(x - x') \Theta(x - x'') = a - \max(x', x'') = \min(a - x', a - x'')$. The constraint of a constant total current is expressed as

$$I_{tot} = \int_0^a dx J(x). \tag{16}$$

In a discretized description [Fig. 2(a)], we denote the "sheet current" $I_i = J(x_i)dx$ with $i = 1$ to N ($i = 1$ is the furthest from the surface; $i = N$ is the closest to the surface), and write the magnetic energy as

$$\begin{aligned} E_B[J(x)] &= \frac{\mu_0}{2}\int_0^a dx' \int_0^a dx'' \frac{I(x')}{dx}\frac{I(x'')}{dx}\min(a-x', a-x'') \\ &\to \frac{1}{2}\sum_{i,j=1}^{N} I_i L_{ij}^{(slab)} I_j. \end{aligned} \tag{17}$$

Identifying $\int_0^a dx' \frac{I(x')}{dx} \to \sum_{i=1}^N \frac{I_i}{dx} dx = \sum_i I_i$ and noting $\min(a-x', a-x'') \to \Delta x \cdot \min(N-i+1, N-j+1)$, the $N \times N$ inductance matrix L is given by $L_{ij}^{(slab)} = \mu_0 \Delta x \cdot \min(N-i+1, N-j+1)$. The inductance matrix in matrix form is

$$L^{(slab)} = \mu_0 \Delta x \begin{bmatrix} N & N-1 & N-2 & \dots & 1 \\ N-1 & N-1 & N-2 & \dots & 1 \\ N-2 & N-2 & N-2 & \dots & 1 \\ \vdots & \vdots & \vdots & \dots & 1 \\ 1 & 1 & 1 & \dots & 1 \end{bmatrix}. \tag{18}$$

In deriving the inductance matrix, we only compute the magnetic energy inside the slab ($x < a$). The magnetic energy outside the SC slab ($x > a$) is proportional to I_{tot}^2, and would shift all components in L by a constant if taken into account. This constant, albeit infinite, can be neglected and does not affect the final results of Eqs. (1).

Minimizing the magnetic energy with the constraints of a given total current of I_{tot} and $|I_n| < I_c$ (sheet current is smaller than some critical current I_c), we find that the SC current fills outer sheets and penetrates only as far as needed to carry I_{tot}. For example, if $I_{tot} = 3.5 I_c$, the solution is $I_N = I_{N-1} = I_{N-2} = I_c$, $I_{N-3} = 0.5 I_c$, and $I_{n<N-3} = 0$ [see the illustration in Fig. 2(c)]. This current distribution is consistent with the Bean model, but it is only a static calculation. In particular, it does not tell how this distribution is reached, and cannot describe the dynamical phenomena such as the hysteresis and the charging process. The dynamics will be addressed in Section III C.

B. Heat due to the reduction of critical current

For a SC slab composed of N sheets carrying a constant total current, $\sum_{n=1}^N \dot{i}_n = 0$. Assuming each sheet has a resistance r_i and $r_1 = 0$ (because the 1st sheet is the furthest from the slab surface), the dynamical equations [Eq. (9)] can be written as

$$\begin{bmatrix} L_{N\times N}^{(slab)} & e_{N\times 1} \\ e_{1\times N}^t & 0 \end{bmatrix} \begin{bmatrix} \dot{i}_1 \\ \dot{i}_2 \\ \vdots \\ \dot{i}_N \\ -\alpha \end{bmatrix} = - \begin{bmatrix} 0 \\ r_2 i_2 \\ \vdots \\ r_N i_N \\ \frac{di_{tot}}{dt} (=0) \end{bmatrix}. \tag{19}$$

In Eq. (19), we consider a uniform filament current and denote $\alpha = v_0'(x)$. $L_{N\times N}^{(slab)} = L^{(slab)}$ is given in Eq. (18); the subscripts are used to denote the matrix size. The difference between the first and

second components in Eq. (19) gives $\dot{i}_1 = r_2 i_2$. Defining an $(N-1)\times(N-1)$ matrix $L_{sub}^{(slab)}$ as

$$L_{sub}^{(slab)} = \mu_0 \Delta x \begin{bmatrix} N-1 & N-2 & \dots & 1 \\ N-2 & N-2 & \dots & 1 \\ \vdots & \vdots & \dots & 1 \\ 1 & 1 & \dots & 1 \end{bmatrix}, \tag{20}$$

Eq. (19) becomes

$$L_{sub}^{(slab)} \begin{bmatrix} \dot{i}_2 \\ \dot{i}_3 \\ \vdots \\ \dot{i}_N \end{bmatrix} + \begin{bmatrix} N-1 \\ N-2 \\ \vdots \\ 1 \end{bmatrix} \dot{i}_1 = - \begin{bmatrix} r_2 i_2 \\ r_3 i_3 \\ \vdots \\ r_N i_N \end{bmatrix} + r_N i_N \begin{bmatrix} 1 \\ 1 \\ \vdots \\ 1 \end{bmatrix}. \tag{21}$$

Using $\dot{i}_1 = r_2 i_2$ and a matrix representation, we get

$$L_{sub}^{(slab)} \begin{bmatrix} \dot{i}_2 \\ \dot{i}_3 \\ \dot{i}_4 \\ \vdots \\ \dot{i}_{N-1} \\ \dot{i}_N \end{bmatrix} = - \begin{bmatrix} N & 0 & 0 & \dots & 0 & -1 \\ N-2 & 1 & 0 & \dots & 0 & -1 \\ N-3 & 0 & 1 & \dots & 0 & -1 \\ \vdots & \vdots & \vdots & \dots & 0 & -1 \\ 2 & 0 & 0 & \dots & 1 & -1 \\ 1 & 0 & 0 & \dots & 0 & 0 \end{bmatrix} \begin{bmatrix} r_2 i_2 \\ r_3 i_3 \\ r_4 i_4 \\ \vdots \\ r_{N-1} i_{N-1} \\ r_N i_N \end{bmatrix} \equiv -X \begin{bmatrix} r_2 i_2 \\ r_3 i_3 \\ r_4 i_4 \\ \vdots \\ r_{N-1} i_{N-1} \\ r_N i_N \end{bmatrix}. \tag{22}$$

Note X is *dimensionless* and has no r_i dependence. The heat can be computed using Eq. (12) (with $r_1 = 0$). Defining $X^{-1} L_{sub}^{(slab)} \equiv \tilde{L}_{sub}^{(slab)}$,

$$\begin{aligned} Q^{(slab)} &= \int dt\, P_L(t) = \int_0^\infty dt \begin{bmatrix} i_2 & i_3 & \dots & i_N \end{bmatrix} \begin{bmatrix} r_2 i_2 \\ \vdots \\ r_N i_N \end{bmatrix} \\ &= - \int_0^\infty dt \begin{bmatrix} i_2 & i_3 & \dots & i_N \end{bmatrix} \tilde{L}_{sub}^{(slab)} \begin{bmatrix} \dot{i}_2 \\ \vdots \\ \dot{i}_N \end{bmatrix} \\ &= - \int_0^\infty dt \frac{d}{dt} \left[\frac{1}{2} \sum_{i=1}^{N-1} \tilde{L}_{sub,ii}^{(slab)} i_{i+1}^2 + \sum_{i=1}^{N-1} \sum_{j=i+1}^{N-1} \tilde{L}_{sub,ij}^{(slab)} i_{i+1} i_{j+1} \right] \\ &\equiv Q^{(slab)}(\{i\}_{\text{initial}}) - Q^{(slab)}(\{i\}_{\text{final}}), \end{aligned} \tag{23}$$

with $Q^{(slab)}(\{i\}) = \frac{1}{2}\sum_{i=1}^{N-1} \tilde{L}_{sub,ii}^{(slab)} i_{i+1}^2 + \sum_{i=1}^{N-1}\sum_{j=i+1}^{N-1} \tilde{L}_{sub,ij}^{(slab)} i_{i+1} i_{j+1}$. $X^{-1} L_{sub}^{(slab)} = \tilde{L}_{sub}^{(slab)}$ can be computed:

$$\tilde{L}_{sub}^{(slab)} = \mu_0 \Delta x \begin{bmatrix} 1 & 1 & 1 & \dots & 1 \\ 1 & 2 & 2 & \dots & 2 \\ 1 & 2 & 3 & \dots & 3 \\ \vdots & \vdots & \vdots & \dots & \vdots \\ 1 & 2 & 3 & \dots & N-2 \\ 1 & 2 & 3 & \dots & N-1 \end{bmatrix}. \tag{24}$$

As an example, for $N=4$, $L_{sub}^{(slab)}$ and $\tilde{L}_{sub}^{(slab)}$ are both 3×3 matrices:

$$L_{sub}^{(slab)}(N=4)=\mu_0\Delta x\begin{bmatrix}3&2&1\\2&2&1\\1&1&1\end{bmatrix},\tilde{L}_{sub}^{(slab)}(N=4)=\mu_0\Delta x\begin{bmatrix}1&1&1\\1&2&2\\1&2&3\end{bmatrix}.$$

Eq. (23) implies that the total heat depends only on initial and final current distributions, but not on the longitudinal resistances. The time to change from the initial to the final current distribution does, however, depend on the longitudinal resistances.

More generally, for an inductance matrix of the "layered structure", the following relation holds:

$$L=\begin{bmatrix}L_1&L_2&L_3&...&L_N\\L_2&L_2&L_3&...&L_N\\L_3&L_3&L_3&...&L_N\\\vdots&\vdots&\vdots&...&L_N\\L_N&L_N&L_N&...&L_N\end{bmatrix}\Rightarrow\tilde{L}_{sub}=\begin{bmatrix}L_1-L_{N-1}&L_1-L_{N-1}&...&L_1-L_{N-1}\\L_1-L_{N-1}&L_1-L_{N-2}&...&L_1-L_{N-2}\\\vdots&\vdots&...&\vdots\\L_1-L_{N-1}&L_1-L_{N-2}&...&L_1-L_N\end{bmatrix}. \tag{25}$$

We have assumed $L_1>L_2>...>L_N$. The inductance matrix has to be symmetric, i.e., $L_{ij}=L_{ji}$, and the layered structure further imposes $L_{ij}=L_{kk}$ with $k=\max(i,j)$. $L^{(slab)}$ defined in Eq. (18) has this structure. To specify the matrix of layered structure, only diagonal components are needed. Eq. (25) indicates that adding a constant to *all* components of inductance matrix does not change the amount of generated heat, as it is their differences, $\tilde{L}_{sub}$, that matter [see the discussion in Section II B].

Now we consider the case where $J_2=J_3=J_4=..=J_N=J$ [Fig. 2(a) and (c)]. With $I_i=J_i\Delta x$ and $\Delta x=a/N$, we get

$$Q(J)=J^2\mu_0(\Delta x)^3\left[\frac{1}{2}\sum_{n=1}^{N-1}n+\sum_{n=1}^{N-1}n(N-n)\right]\underset{N\to\infty}{\to}J^2\mu_0\frac{a^3}{6}. \tag{26}$$

The first summation $(\Delta x)^3\sum_{n=1}^{N-1}n$ comes from the diagonal components, and approaches zero in $N\to\infty$ limit; the second summation $(\Delta x)^3\left[\sum_{n=1}^{N-1}n(N-n)\right]$ comes from all off-diagonal components, and approaches $\int_0^a dx\,x(a-x)=a^3/6$ in $N\to\infty$ limit. The total generated heat from $J_i=J$ to $J_i=J-\Delta J$ is

$$Q(J)-Q(J-\Delta J)=\mu_0 J\Delta J\frac{a^3}{3}, \tag{27}$$

identical to that obtained from a direct slab calculation (see Eq.(7.3) in Ref.[3]).

Finally, we point out the "layered structure" of inductance matrix [Eq. (25)] implies that the current injection starts at the Nth filament, and then $(N-1)$th, ... etc. This can be understood as follows. When the inter-filament resistance is small (which is usually the case), all filaments tend to have the same potential drop. When there is no resistance, the dynamical equation is simply $v_0|e\rangle=L\frac{d\mathbf{i}}{dt}$ subject to a current injection rate $\frac{di_{tot}}{dt}$. By subtracting adjacent components of this vector equation, we get $\frac{di_N}{dt}=\frac{di_{tot}}{dt}$, indicating only the current of the Nth filament is increasing. Once the Nth filament reaches its critical current, $i_N\sim i_c$ and $\frac{di_N}{dt}=0$. We can solve the same $v_0|e\rangle=L\frac{d\mathbf{i}}{dt}$ but with $\frac{di_N}{dt}=0$. Following the same procedure we get $\frac{di_{N-1}}{dt}=\frac{di_{tot}}{dt}$, indicating the only the current of the $(N-1)$th filament is increasing. This process will continue until all filaments reach their critical currents. We recognize that this is the characteristic behavior of the Bean model (i.e., the current change starts at the surface) and will show the circuit model simulation in Section III C (next subsection).

C. Circuit model simulation of current injection

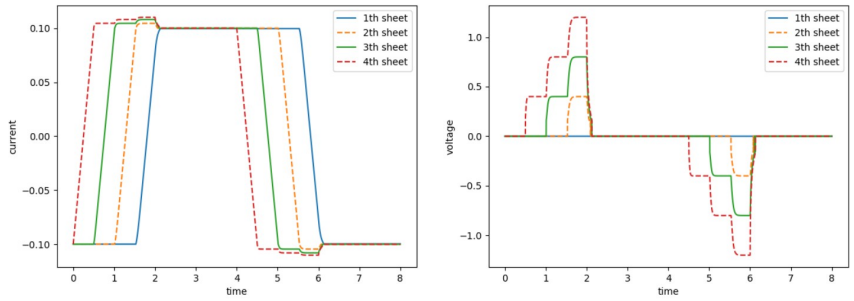

FIG. 3. The charging process of 4 SC filaments, using the inductance matrix of a SC slab composed of four SC sheets. The change of input current always affects the outermost sheet (i.e., the 4th sheet) first, and then propagate deeper inside the SC slab. The critical current $I_c = 0.1$ in this simulation. (a) The current distribution as a function of time. (b) The sheet voltage, in the unit of μ_0, as a function of time: a staircase behavior is observed.

To simulate the current injection in the circuit model, we consider a given initial current distribution with a constant positive current injection rate $\dot{I}_{tot}$; we then ask the current distribution $I_i(t)$. To be concrete, we take $N = 4$ with the inductance matrix:

$$L = \mu_0 \begin{bmatrix} 4 & 3 & 2 & 1 \\ 3 & 3 & 2 & 1 \\ 2 & 2 & 2 & 1 \\ 1 & 1 & 1 & 1 \end{bmatrix} . \tag{28}$$

This inductance matrix models the SC slab as four successive SC sheets. 4 corresponds to the outermost sheet (i.e., the interface between the SC slab and the vacuum); 1 corresponds to the deepest sheet (furthest away from the interface) [see Eq. (18)]. In the simulation, the non-linear resistance is specified by $r_0 = 10^{-6}$, $I_c = 0.1$, and $n = 20$ in Eq. (11), and "inter-sheet" conductance by $g_{ij} = 10^6$ for $i \neq j$ for $\mathbf{g}$ defined in Eq. (3c). The current injection is given by

$$\frac{dI_{tot}}{dt} = \dot{I}_{tot} = \begin{cases} 0.4 & 0 < t < 2 \\ 0 & 2 < t < 4 \text{ and } t > 6 \\ -0.4 & 4 < t < 6 \end{cases} . \tag{29}$$

Current of $0.8\, I_c$ is injected during $t = 0$ to 2; the same amount of current is removed during $t = 4$ to 6. The initial condition is $I_1 = I_2 = I_3 = I_4 = -I_c = -0.1$. The current distribution as a function of time is shown in Fig. 3(a). We see that with this form of inductance matrix, the current of 4th (closest to the surface) sheet changes from $-I_c$ to $+I_c$ first, then the 3rd, then the 2nd, and finally the 1st. When reversing the current source, the current of the 4th sheet changes from $+I_c$ to $-I_c$ first, then the 3rd, then the 2nd, and finally the 1st. This order is expected from the Bean model (i.e., the change starts at the surface) and accounts for the hysteresis behavior. In the circuit model, this behavior originates from the "layered" structure of induction matrix (see Section III B).

When there is no resistance ($I_n < I_c$ for all n), the current change is completely determined by the inductance and the time derivative of the sheet currents, but has nothing to do with values of sheet currents. When some of the filaments develop a non-zero resistance, the currents on these sheets saturate around I_c and the remaining current flows through the sheets whose currents are smaller than I_c.

Fig. 3(b) shows the voltage distribution (computed by $v_n(t) = r_n \cdot i_n(t)$) as a function of time, and the staircase behavior can be understood as follows. When there is no resistance, Eq. (9) implies $\mathbf{v}(t) = -L\frac{d\mathbf{i}}{dt} + \alpha(t)$. During the current injection, $\frac{d\mathbf{i}}{dt}$ goes through four phases:

$$\frac{d\mathbf{i}}{dt} = \begin{bmatrix} 0 \\ 0 \\ 0 \\ \dot{I}_{tot} \end{bmatrix} \rightarrow \begin{bmatrix} 0 \\ 0 \\ \dot{I}_{tot} \\ 0 \end{bmatrix} \rightarrow \begin{bmatrix} 0 \\ \dot{I}_{tot} \\ 0 \\ 0 \end{bmatrix} \rightarrow \begin{bmatrix} \dot{I}_{tot} \\ 0 \\ 0 \\ 0 \end{bmatrix}. \tag{30}$$

Each phase lasts a period of $2I_c/\dot{I}_{tot} (= 2 \times 0.1/0.4 = 0.5$ in this simulation). The corresponding voltages for these four phases are

$$\mathbf{v}(t) = -\mu_0 \begin{bmatrix} 1 \\ 1 \\ 1 \\ 1 \end{bmatrix} \dot{I}_{tot} + \alpha_1 \rightarrow -\mu_0 \begin{bmatrix} 2 \\ 2 \\ 2 \\ 1 \end{bmatrix} \dot{I}_{tot} + \alpha_2 \rightarrow -\mu_0 \begin{bmatrix} 3 \\ 3 \\ 2 \\ 1 \end{bmatrix} \dot{I}_{tot} + \alpha_3 \rightarrow -\mu_0 \begin{bmatrix} 4 \\ 3 \\ 2 \\ 1 \end{bmatrix} \dot{I}_{tot} + \alpha_4. \tag{31}$$

$\alpha_i(t)$ is determined by requiring the zero voltage in the innermost sheet as the deepest sheet experiences no flux change and thus no voltage. With this input, we get $\alpha_1 = \mu_0 \dot{I}_{tot}$, $\alpha_2 = 2\mu_0 \dot{I}_{tot}$, $\alpha_3 = 3\mu_0 \dot{I}_{tot}$, and $\alpha_4 = 4\mu_0 \dot{I}_{tot}$, from which the voltage sequence turns out to be

$$\mathbf{v}(t) = \mu_0 \begin{bmatrix} 0 \\ 0 \\ 0 \\ 0 \end{bmatrix} \dot{I}_{tot} \rightarrow \mu_0 \begin{bmatrix} 0 \\ 0 \\ 0 \\ 1 \end{bmatrix} \dot{I}_{tot} \rightarrow \mu_0 \begin{bmatrix} 0 \\ 0 \\ 1 \\ 2 \end{bmatrix} \dot{I}_{tot} \rightarrow \mu_0 \begin{bmatrix} 0 \\ 1 \\ 2 \\ 3 \end{bmatrix} \dot{I}_{tot}. \tag{32}$$

If we look at the voltage at 4th sheet $v_4(t)$, it goes from 0 to $\mu_0 \dot{I}_{tot}$ to $2\mu_0 \dot{I}_{tot}$ to $3\mu_0 \dot{I}_{tot}$, consistent with Fig. 3(b) which is obtained by directly solving the Eq. (1). We have numerically checked the plateau values are *independent* of the resistance $r(I)$. The current at each sheet saturates at a value slightly larger than I_c, and the exact amount depends on the longitudinal resistance $r(I)$. For this reason, the heat generation rate, computed by $I_n \cdot v_n$, in principle depends on r. However, if $r_n(I)$ increases sufficiently fast so that $I \sim I_c$ can accumulate any voltage, the generated heat becomes independent of $r(I)$, which is the ideal case considered in the typical continuum medium calculation[3].

We can now consider the heat generated by a constant injection rate $\dot{I}_{tot}$. Let us give the heat generation in a continuum SC slab over the period when I_{tot} changes from $J_c a$ to $-J_c a$, as illustrated in Fig. 2(c). The total heat is computed by

$$\begin{aligned} \Delta\phi(x) &= \int_0^x dx' \, \Delta B(x') = \int_0^x dx' \, 2\mu_0 J_c x' = \mu_0 J_c x^2, \\ Q_{slab} &= \int_0^a dx J_c \Delta\phi(x) = \int_0^a dx \mu_0 J_c^2 x^2 = \mu_0 J_c^2 \frac{a^3}{3}. \end{aligned} \tag{33}$$

$\Delta\phi(x)$ is the change of magnetic flux at x, and $\Delta B(x') = 2\mu_0 J_c x'$ is the change of magnetic field when the current density goes from $+J_c$ to $-J_c$ as shown in the green curve in Fig. 2(a). Eq. (33)

(see Eq.(8.5) in Ref.[3]) shall be reproduced in the circuit model calculation in the infinite-sheet limit.

In the circuit model, if we (i) identify $J_n = I_n/(\Delta x)$, (ii) neglect the transient behavior of $v_n(t)$, and (iii) assume the current density is J_c, the generated heat can be computed as

$$\begin{aligned} Q_{cir} &= \mu_0 2 J_c^2 (\Delta x)^3 \sum_{n=1}^{N} \left[\sum_{j=1}^{n} j \right] = \mu_0 2 J_c^2 (\Delta x)^3 \sum_{n=1}^{N} \frac{n(n+1)}{2} \\ &\underset{n\Delta x = x_n}{\to} 2 J_c^2 \mu_0 (\Delta x) \sum_{n=1}^{N} \frac{x_n^2}{2} \underset{N\to\infty}{\to} \mu_0 J^2 \frac{a^3}{3}. \end{aligned} \tag{34}$$

In the $N \to \infty$ limit, $Q_{cir} = Q_{slab}$. In our circuit model simulation, there is still a weak r-dependence because our choice of $r(I)$ does not increase fast enough when $I > I_c$.

In this section, we have demonstrated that the circuit model can simulate the current distribution and heat generation during the current injection. The results are fully consistent with the Bean model. In fact, the circuit model provides more information – the dynamical or transient behavior – which the Bean model does not include in the first place. We shall comment on the relation between the Bean model and the circuit model more in Section IV D. The inductance matrix plays the crucial role in the dynamics. After all, when the resistance is zero, the inductance completely determines how currents change in time.

IV. SUPERCONDUCTING CYLINDER OF STRAIGHT FILAMENTS

In this section we consider a SC cylinder composed of straight filaments as illustrated in Fig. 2(b). Cylinder serves as the idealized geometry of a SC wire. The straight filaments imply that the SC current only flows along the axial direction. We will model the SC wire as a collection of concentric shells and determine its self and mutual inductances by computing the magnetic energy. The results obtained in this section will be used in Section V where the filaments are twisted. The heat generated by (i) reduction of I_c with total current fixed and (ii) the change of total current will be computed.

A. SC cylinder as concentric shells - inductance matrix

For a SC cylinder of radius R with a current density distribution $J(r)$, the magnetic field inside the cylinder is given by

$$\begin{aligned} &B(r) 2\pi r = \mu_0 \int_0^r dr' J(r') 2\pi r' \\ &\Rightarrow B(r) = \frac{\mu_0}{r} \int_0^r dr' J(r') r' = \frac{\mu_0}{r} \int_0^R dr' J(r') r' \Theta(r - r'). \end{aligned} \tag{35}$$

The total magnetic energy for $r < R$ is given by

$$\begin{aligned} E_B[J(r)] &= \frac{1}{2\mu_0}\int_0^R dr\,|B(r)|^2 2\pi r = \mu_0\pi\int_0^R dr\,\frac{1}{r}\left[\int_0^R dr'\,J(r')r'\Theta(r-r')\right]^2 \\ &= \mu_0\pi\int_0^R dr'\int_0^R dr''\,J(r')J(r'')r'r''\left[\int_0^R dr\,\frac{1}{r}\Theta(r-r')\Theta(r-r'')\right] \\ &= \mu_0\pi\int_0^R dr'\int_0^R dr''\,J(r')J(r'')r'r''\left[\int_{\max(r',r'')}^R dr\,\frac{1}{r}\right] \\ &= \mu_0\pi\int_0^R dr'\int_0^R dr''\,J(r')J(r'')r'r''\log\left[\frac{R}{\max(r',r'')}\right], \end{aligned} \tag{36}$$

with a total current $I_{tot} = \int_0^R dr J(r) 2\pi r$. The last two expressions are identical; we can choose either depending on our convenience. The magnetic energy for $r > R$ will be neglected as it only introduces a (infinite) constant to all components of the inductance matrix.

Now we discretize [Fig. 2(b)] the cylinder of radius R into N concentric shells, so r is defined at $r_i = \Delta r \cdot i$ and the function $J(r)$ is parameterized by $J_1 = J(r_1)$, $J_2 = J(r_2)$, ..., $J_N = J(r_N)$. Let us introduce I_i to be the current between r_{i-1} and r_i (i.e., the current of ith shell) so that $I_i = 2\pi r_i J_i \Delta r$. Using the shell current as the variables, the magnetic energy becomes

$$E_B[I(r)] = \frac{\mu_0}{4\pi}\int_0^R dr'\int_0^R dr''\,\frac{I(r')}{\Delta r}\frac{I(r'')}{\Delta r}\log\frac{R}{\max(r',r'')} \to \frac{1}{2}\sum_{ij=1}^{N} I_i L_{ij}^{(cyl)} I_j, \tag{37}$$

subject to the constraint $\sum_{i=1}^N I_i = I_{tot}$. L is identified as the inductance matrix (both self and mutual) between concentric shells. For $N = 5$, the inductance matrix has the form

$$L^{(cyl)} = \frac{\mu_0}{2\pi}\begin{bmatrix} \log[R/r_1] & \log[R/r_2] & \log[R/r_3] & \log[R/r_4] & \log[R/r_5] \\ \log[R/r_2] & \log[R/r_2] & \log[R/r_3] & \log[R/r_4] & \log[R/r_5] \\ \log[R/r_3] & \log[R/r_3] & \log[R/r_3] & \log[R/r_4] & \log[R/r_5] \\ \log[R/r_4] & \log[R/r_4] & \log[R/r_4] & \log[R/r_4] & \log[R/r_5] \\ \log[R/r_5] & \log[R/r_5] & \log[R/r_5] & \log[R/r_5] & \log[R/r_5] \end{bmatrix}. \tag{38}$$

This inductance matrix shares the same "layered structure" as Eq. (25).

B. Heat due to the reduction of critical current

The Joule heating can be computed using the same procedure in Section III B, with the inductance matrix replaced by $L^{(cyl)}$. Following the same procedure, the diagonal components of $\tilde{L}_{sub}^{(cyl)}$ are

$$\tilde{L}_{sub,diag}^{(cyl)} = \frac{\mu_0\Delta r}{2\pi}\left[\textstyle\sum_{i=1}^{1}\frac{1}{r_i},\ \sum_{i=1}^{2}\frac{1}{r_i},\ \cdots\ \sum_{i=1}^{N-2}\frac{1}{r_i},\ \sum_{i=1}^{N-1}\frac{1}{r_i}\right], \tag{39}$$

and $\tilde{L}_{sub,ij}^{(cyl)} = \tilde{L}_{sub,kk}^{(cyl)}$ with $k = \min(i,j)$. Comparing to the continuum medium, we identify $r_1 = c$ and $r_N = R$ over which the SC current flows. For a constant current density, $I_i = J_c 2\pi r_i \Delta r$ and we

obtain

$$
\begin{aligned}
Q^{(cyl)}(J_c) &= \frac{\mu_0 \Delta r}{2\pi} \sum_{n=1}^{N} \left[\sum_{i=1}^{n} \frac{1}{r_n} \right] I_n \left[\sum_{j=n+1}^{N} I_j \right] \\
&= \frac{\mu_0}{2\pi} (2\pi)^2 (\Delta r) J_c^2 \sum_{n=1}^{N} \left[(\Delta r) \sum_{i=1}^{n} \frac{1}{r_n} \right] r_n \left[(\Delta r) \sum_{j=n+1}^{N} r_j \right] \\
(r_n \to r) &\to 2\pi\mu_0 J_c^2 \int_c^R dr \left[\log \frac{r}{c} \right] r \left[\frac{1}{2}(a^2 - r^2) \right] \\
&= \frac{\pi\mu_0 J_c^2}{2} R^4 \left[-\frac{3}{8} + \frac{\varepsilon^2}{2} - \frac{\varepsilon^4}{8} - \frac{\log \varepsilon}{2} \right],
\end{aligned}
\tag{40}
$$

with $\varepsilon = \frac{c}{R}$. The total heat per unit area is given by

$$
\frac{Q^{(cyl)}(J_c) - Q^{(cyl)}(J_c - \Delta J_c)}{\pi R^2} = \mu_0 R^2 J_c \Delta J_c \left[-\frac{3}{8} + \frac{\varepsilon^2}{2} - \frac{\varepsilon^4}{8} - \frac{\log \varepsilon}{2} \right]. \tag{41}
$$

This result is identical to the direct calculation of a SC cylinder (see Eq.(7.11) in Ref.[3]).

C. Heat due to the changing total current

Now we consider the case where the total current is changing in time. The total heat per unit cross section is computed by

$$
\begin{aligned}
Q^{(cyl,2)} &= \frac{4}{\pi R^2} \int_c^R dr\, 2\pi r J_c \Delta\phi(r) = \frac{4\mu_0 J_c^2}{R^2} \int_c^R dr \left[\frac{r^3}{2} - \frac{c^2 r}{2} - c^2 r \log \frac{r}{c} \right] \\
&= \frac{\mu_0 J_c^2 R^2}{2} \left[(1-\varepsilon^2)^2 - 2\varepsilon^2(-1 + \varepsilon^2 - 2\log\varepsilon) \right] = \frac{\mu_0 J_c^2 R^2}{2} \left[1 - \varepsilon^4 + 4\varepsilon^2 \log\varepsilon \right],
\end{aligned}
\tag{42}
$$

with $\varepsilon = \frac{c}{R}$. We identify $B(r) = \frac{\mu_0 J_c}{2} \left[r - \frac{c^2}{r} \right]$ and $\Delta\phi(r) = \int_c^r dr' B(r') = \frac{\mu_0 J_c}{2} \left[\frac{r^2}{2} - \frac{c^2}{2} - c^2 \log \frac{r}{c} \right]$ when the current density changes from J_c to zero (see Eq.(8.92) in Ref.[3]). Eq. (42) will be reproduced in the circuit model calculation shortly.

For the circuit model, we consider the problem where the currents change from $I_i = 2\pi r_i J_c \Delta r$ to $I_i = 0$, for $i = 1$ to N. Because the building blocks are concentric shells in a SC cylinder and they have different spatial size, the critical currents of building blocks are different. Following the discussion in Section III C, we compute the flux change by $\Delta\phi = \mathbf{v}\Delta t = -L^{(cyl)} \cdot \Delta \mathbf{I}_{tot} + \alpha(t)$, with the offset $\alpha(t)$ fixed by requiring that the inner-most shell has no flux change. Let us use $N = 4$ as a concrete example. Due to the "layered structure" of $L^{(cyl)}$ [Eq. (38) for example], the current change starts with the 4th shell, then the 3rd, then the 2nd, and finally the 1st (see Section III B). Because each shell carries a current of $2\pi r_i J_c \Delta r = \Delta I_i$, the corresponding flux change during these

four phases is

$$\begin{aligned}\Delta\phi = -L^{(cyl)}\begin{bmatrix}0\\0\\0\\2\pi r_4 J_c\Delta r\end{bmatrix} + \alpha_1 \to -L^{(cyl)}\begin{bmatrix}0\\0\\2\pi r_3 J_c\Delta r\\0\end{bmatrix} + \alpha_2 \\ \to -L^{(cyl)}\begin{bmatrix}0\\2\pi r_2 J_c\Delta r\\0\\0\end{bmatrix} + \alpha_3 \to -L^{(cyl)}\begin{bmatrix}2\pi r_1 J_c\Delta r\\0\\0\\0\end{bmatrix} + \alpha_4.\end{aligned} \tag{43}$$

Fixing α_i by requiring a zero flux change in the innermost shell, we get

$$\frac{\Delta\phi}{\mu_0 J_c} = \begin{bmatrix}0\\0\\0\\0\end{bmatrix} \to (\Delta r)^2\begin{bmatrix}0\\0\\0\\r_4\frac{1}{r_4}\end{bmatrix} \to (\Delta r)^2\begin{bmatrix}0\\0\\r_3\frac{1}{r_3}\\r_3(\frac{1}{r_3}+\frac{1}{r_4})\end{bmatrix} \to (\Delta r)^2\begin{bmatrix}0\\r_2\frac{1}{r_2}\\r_2(\frac{1}{r_3}+\frac{1}{r_4})\\r_2(\frac{1}{r_2}+\frac{1}{r_3}+\frac{1}{r_4})\end{bmatrix}. \tag{44}$$

For the 4th strand, the flux changes from 0 to $\mu_0 J_c(\Delta r)^2 r_4\frac{1}{r_4}$, to $\mu_0 J_c(\Delta r)^2 r_3(\frac{1}{r_3}+\frac{1}{r_4})$, and finally to $\mu_0 J_c(\Delta r)^2 r_2(\frac{1}{r_2}+\frac{1}{r_3}+\frac{1}{r_4})$. Generally for nth shell, the voltage is given by

$$\Delta\phi_n = \mu_0 J_c(\Delta r)^2\sum_{m=1}^{n} r_m\left[\sum_{i=m}^{n}\frac{1}{r_i}\right]. \tag{45}$$

The total heat is computed by $\mathbf{I}^T\Delta\phi$. For $N=4$, $\mathbf{I}^T = 2\pi J_c\Delta r(r_1,r_2,r_3,r_4)$. Denoting $r_1 = c$ and $r_N = R$, the total generated heat is $\sum_{n=1}^{N} 2\pi J_c\Delta r r_n\cdot\Delta\phi_n$, leading to

$$\begin{aligned}Q_{cir}^{(cyl,2)} &= 4\times\frac{2\pi J_c^2\mu_0}{\pi R^2}(\Delta r)^3\sum_{n=1}^{N} r_n\sum_{m=1}^{n} r_m\left[\sum_{i=m}^{n}\frac{1}{r_i}\right] \\ &\quad \text{identify } r_m = r', r_n = r, \text{ and } \sum_{i=m}^{n}\frac{1}{r_i}\Delta r = \log\frac{r}{r'} \\ &\to \frac{8J_c^2\mu_0}{R^2}\int_c^R dr\, r\int_c^r dr'\, r'\log\frac{r}{r'} = \frac{8J_c^2\mu_0}{R^2}\frac{R^4}{16}\left[1-\varepsilon^4+4\varepsilon^2\log\varepsilon\right] \\ &= \frac{J_c^2\mu_0 R^2}{2}\left[1-\varepsilon^4+4\varepsilon^2\log\varepsilon\right].\end{aligned} \tag{46}$$

Compared to Eq. (42), we find $Q_{cir}^{(cyl,2)} = Q^{(cyl,2)}$ as it should be.

In this section, we have shown that a SC cylinder can be described by a collection of concentric shells which are the building blocks of the circuit model. The inductance matrix, obtained by computing the magnetic energy, possesses the same "layered structure" as the SC slab. As discussed in Section III B, this structure leads to the behavior where the current change starts at the surface. The heat generated current redistribution, either by reduction of critical current or by changing the total current, approaches the Bean-model results when the number of shells becomes infinite.

D. Relation between the Bean model and the circuit model

We close this section by arguing that the circuit model is a more complete description of the system, and the Bean model can be regarded as a simplified or coarse-grained version of the circuit model. This argument is based on the following two observations. First, the Bean model is quasi-static, and cannot describe the time-dependent processes completely. The circuit model, on the other hand, is dynamical and is able to fully describe the system responses to the time-varying external perturbations[20,41]. Second, the Bean model is mainly used to describe a continuum of SC material of high symmetry, whereas the circuit model allows for the discontinuous SC structure. Therefore, by taking the proper limit the circuit model can (and should) reproduce the results of the Bean model, but it is not obvious how the Bean model can be directly applied to system of composite SC materials[42].

To illustrate the validity of the circuit model and that of the Bean model, we consider the heat generation during the external time-varying perturbation. In Sections III B, III C, IV B, IV C, the heat generation using the circuit model is computed. To exactly match the heat generation computed by the Bean model, we need to take the index number n defined in Eq. (10) to be infinite. Therefore, in terms of heat generation, the Bean model is a good approximation for high-quality superconductors only, but the circuit model can deal with superconductors of any qualities. As the amount of heat is crucial for determining the quench condition[3], the circuit model can provide some correction the quench current determined using the Bean model. However, since one is usually interested in high-quality SC, this correction is usually small.

V. SUPERCONDUCTING WIRE OF TWISTED FILAMENTS

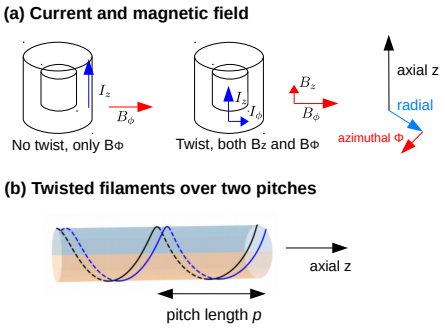

FIG. 4. (a) Illustration of the twisted SC filaments that form a SC wire. Without twisting, current only flows along z and therefore only B_ϕ is non-zero. Once strands are twisted, both I_z and I_ϕ components are present, therefore both B_z and B_ϕ are non-zero. (b) Two close twisted filaments over two pitch lengths.

Now we consider the SC wire of twisted filaments. In Ref.[43], Turck showed that the twisted filaments can induce a small uniform current inside the SC wire. We see how this is obtained in the circuit model.

A. Main results in Ref.[43]

We recapitulate a few results in Ref.[43]. The problem is to compute the magnetic field distribution between layers of twisting filaments with pitch length p. The key physics is that *the total magnetic flux between two twisted filaments, over one pitch, is zero*, because there is no electric field inside each SC filament. This requirement determines the magnetic field and the current distributions. Two ingredients of this calculation are (i) the magnetic field; and (ii) the area enclosed by two twisted filaments.

Following Ref.[43], $I(r)$ is denoted as the total current inside a cylinder of radius r. We consider the twisted pitch p is much larger than the radius of the cylinder, and get

$$\frac{J_\phi}{J_z} = \frac{2\pi r}{p} \ll 1. \tag{47}$$

Under this condition, the total current density can be approximated J_z and $I(r_1) = \int_0^{r_1} dr\, 2\pi r J_z(r)$. Due to the twisting, the magnetic field has both azimuthal $\hat{\phi}$ and axial $\hat{z}$ components [Fig. 4(a)]. Using Ampere's law,

$$B_\phi(r) = \mu_0 \frac{I(r)}{2\pi r},\ B_z(r) = \frac{\mu_0}{p}\left[I_{tot} - I(r)\right]. \tag{48}$$

To compute the magnetic flux, we also need the area element between two twisted filaments. The trajectory of one twisted filament with twisted pitch p is [Fig. 4(b)]

$$\mathbf{r}_1(r,\phi) = (r\cos\phi, r\sin\phi, \frac{p}{2\pi}\phi). \tag{49}$$

The x, y go back to the original values while z is changed by the twisted pitch p. The area spanned by two nearby strands is given by $\partial_\phi \mathbf{r}_1 d\phi \wedge \partial_r \mathbf{r}_1 dr$, and is computed by

$$\begin{aligned} \partial_\phi \mathbf{r}_1 &= (-r\sin\phi, r\cos\phi, \frac{p}{2\pi}), \\ \partial_r \mathbf{r}_1 &= (\cos\phi, \sin\phi, 0), \\ d\mathbf{a} &= dr\, d\phi\, \left[\partial_\phi \mathbf{r}_1 \wedge \partial_r \mathbf{r}_1\right] = dr\, dz \left[\hat{\phi} - \frac{2\pi r}{p}\hat{z}\right]. \end{aligned} \tag{50}$$

We have used $\hat{r} = (\cos\phi, \sin\phi, 0)$, $\hat{\phi} = (-\sin\phi, \cos\phi, 0)$, $\hat{z} = (0,0,1)$, so that $\hat{z} = \hat{r} \times \hat{\phi}$. By requiring the total flux within a pitch is zero, we get

$$\begin{aligned} &\int_{r_1}^{r_1+e} dr \int_0^{2\pi} d\phi\, B_\phi \frac{p}{2\pi} + \int_{r_1}^{r_1+e} dr \int_0^{2\pi} d\phi\, B_r \times (-r) = 0 \\ \Rightarrow &\int_{r_1}^{r_1+e} dr \frac{I(r)}{r} - \left(\frac{2\pi}{p}\right)^2 \int_{r_1}^{r_1+e} dr\, r[I_{tot} - I(r)] = 0. \end{aligned} \tag{51}$$

Eq. (48) has been used. With e being a small quantity, we approximate $\int_{r_1}^{r_1+e} dr \frac{I(r)}{r} \approx I(r_1)\frac{e}{r_1}$ and $\int_{r_1}^{r_1+e} dr\, r[I_{tot} - I(r)] \approx [I_{tot} - I(r_1)] r_1 e$. To the first order of e we get

$$\begin{aligned} &I(r_1)\frac{e}{r_1} - \left(\frac{2\pi}{p}\right)^2 [I_{tot} - I(r_1)] r_1 e = 0 \\ \Rightarrow &I(r_1) = \frac{4\pi^2 r_1^2}{p^2} I_{tot} \frac{1}{1 + 4\pi^2 r_1^2/p^2} \approx \frac{4\pi^2 r_1^2}{p^2} I_{tot}, \end{aligned} \tag{52}$$

where $p \gg r_1$ is used. The r^2 dependence implies that a constant current density $\frac{4\pi}{p^2} I_{tot}$ inside the SC wire of twisted filaments. This result is given on p.482 of Ref.[43].

B. Inductance matrix caused by twisting

To obtain the inductance matrix, we compute the magnetic energy as a functional of current density distribution $J(r)$ using Eq. (48). The B_ϕ contribution is already derived in Eq. (38):

$$L_{ij}^{(cyl)} = \frac{\mu_0}{2\pi} \log\left[\frac{R}{\max(r_i, r_j)}\right], \tag{53}$$

with $r_i = c + i \cdot \Delta r$. We focus on the B_z contribution:

$$\begin{aligned} E_{mag,z}[J(r)] &= \frac{1}{2\mu_0} \int_0^R dr\, 2\pi r \left[\frac{\mu_0}{p}(I_{tot} - \int_0^r dr'\, 2\pi r' J(r'))\right]^2 \\ &= \frac{\pi\mu_0}{p^2}\left\{\frac{R^2}{2} I_{tot}^2 - 2I_{tot}\int_0^R dr\, r \int_0^r dr'\, 2\pi r' J(r') + \int_0^R dr\, r \left[\int_0^r dr'\, 2\pi r' J(r')\right]^2\right\}. \end{aligned} \tag{54}$$

Three terms in Eq. (54) are evaluated. The first term only involves I_{tot}^2. This term can be neglected, but we keep it to make the final expression [Eq. (58)] simpler. Using $I_{tot} = \int_0^R dr\, 2\pi r J(r)$, we write

$$\begin{aligned} \frac{\pi\mu_0}{p^2}\frac{R^2}{2} I_{tot}^2 &= \mu_0 \frac{\pi R^2}{2p^2}\left[\int_0^R dr'\, 2\pi r' J(r')\right]\left[\int_0^R dr''\, 2\pi r'' J(r'')\right] \\ &= \mu_0 \frac{\pi R^2}{2p^2}\int_0^R dr' \int_0^R dr'' \frac{I(r')}{\Delta r}\frac{I(r'')}{\Delta r} \to \frac{1}{2}\sum_{i,j=1}^N L_{ij}^{(1)} I_i I_j. \end{aligned} \tag{55}$$

Here we used $I_i = I(r_i) = 2\pi r_i J(r_i)\Delta r$. In the discretized description, $\int_0^R dr' \frac{I(r')}{\Delta r} \to \sum_{i=1}^N I_n$ and we find $L_{ij}^{(1)} = \mu_0 \frac{\pi R^2}{p^2}$. Using $\int_0^r dr'\, 2\pi r' J(r') = \int_0^R dr'\, 2\pi r' J(r')\Theta(r - r')$, the third term in Eq. (54) can be written as

$$\begin{aligned} &\frac{\pi\mu_0}{p^2}\int_0^R dr\, r\left[\int_0^R dr'\, 2\pi r' J(r')\Theta(r-r')\right]\left[\int_0^R dr''\, 2\pi r'' J(r'')\Theta(r-r'')\right] \\ &= \frac{\pi\mu_0}{p^2}\int_0^R dr' \int_0^R dr'' \frac{I(r')}{\Delta r}\frac{I(r'')}{\Delta r}\frac{1}{2}\left[R^2 - [\max(r', r'')]^2\right] \to \frac{1}{2}\sum_{i,j=1}^N L_{ij}^{(3)} I_i I_j. \end{aligned} \tag{56}$$

$L_{ij}^{(3)}$ is thus identified as $\frac{\pi\mu_0}{p^2}\left[R^2 - [\max(r_i, r_j)]^2\right]$. For the second term in Eq. (54),

$$\begin{aligned} &-\frac{\pi\mu_0}{p^2}\int_0^R dr\, r\left[\int_0^R dr'\, 2\pi r' J(r') \int_0^R dr''\, 2\pi r'' J(r'')\Theta(r-r'')\right. \\ &\left. + \int_0^R dr''\, 2\pi r'' J(r'') \int_0^R dr'\, 2\pi r' J(r')\Theta(r-r')\right] \\ &= -\frac{\pi\mu_0}{p^2}\int_0^R dr' \int_0^R dr'' \frac{I(r')}{\Delta r}\frac{I(r'')}{\Delta r}\frac{2R^2 - (r'^2 + r''^2)}{2} \to \frac{1}{2}\sum_{i,j=1}^N L_{ij}^{(2)} I_i I_j. \end{aligned} \tag{57}$$

$L_{ij}^{(2)}$ is identified as $-\frac{\pi\mu_0}{p^2}(2R^2 - [r_i^2 + r_j^2])$. Combining all three terms in Eq. (54), we get

$$L_{ij}^{(twist)} = L_{ij}^{(1)} + L_{ij}^{(2)} + L_{ij}^{(3)} = +\frac{\mu_0\pi}{p^2}\left[\min(r_i, r_j)\right]^2. \tag{58}$$

C. Currents of inner shells due to twisting

Now we compute the currents of inner shells due to twisting and show that they are consistent with Eq. (52). Denoting $L_0 = L^{(cyl)}$ and $L_1 = L^{(twist)}$. The linear equation we want to solve is

$$\begin{bmatrix} (L_0+L_1) & e \\ e^t & 0 \end{bmatrix} \begin{bmatrix} \dot{\mathbf{i}} \\ -\alpha \end{bmatrix} = \begin{bmatrix} \mathbf{0} \\ \dot{I}_{tot} \end{bmatrix}, \tag{59}$$

with $e^t = (1,1,1,...1)$. Since $p \gg r$ is assumed [Eq. (47)], $L_0 \gg L_1$ and the perturbation expansion can be used to get the solution. Writing $\dot{\mathbf{i}} = \dot{\mathbf{i}}^{(0)} + \dot{\mathbf{i}}^{(1)}$ and $\alpha = \alpha^{(0)} + \alpha^{(1)}$, the 0th order satisfies

$$\begin{bmatrix} L_0 & e \\ e^t & 0 \end{bmatrix} \begin{bmatrix} \dot{\mathbf{i}}^{(0)} \\ -\alpha^{(0)} \end{bmatrix} = \begin{bmatrix} \mathbf{0} \\ \dot{I}_{tot} \end{bmatrix}. \tag{60}$$

The solution is $\dot{\mathbf{i}}^{(0)} = (0,0,0,...,\dot{I}_{tot})^T$, i.e., only the last component has a non-zero value of $\dot{I}$. The first order quantities satisfy

$$L_0\dot{\mathbf{i}}^{(1)} + L_1\dot{\mathbf{i}}^{(0)} = \alpha^{(1)}e, \text{ or } L_0\dot{\mathbf{i}}^{(1)} = -L_1\dot{\mathbf{i}}^{(0)} + \alpha^{(1)}e, \tag{61}$$

subject to $\sum_{n=1}^{N} \dot{i}_n^{(1)} = 0$. We proceed to use $N = 4$ inductance matrix, but the generalization is straightforward. For $N = 4$, we need to solve

$$\begin{aligned} \frac{\mu_0}{2\pi} \begin{bmatrix} \log[R/r_1] & \log[R/r_2] & \log[R/r_3] & \log[R/r_4] \\ \log[R/r_2] & \log[R/r_2] & \log[R/r_3] & \log[R/r_4] \\ \log[R/r_3] & \log[R/r_3] & \log[R/r_3] & \log[R/r_4] \\ \log[R/r_4] & \log[R/r_4] & \log[R/r_4] & \log[R/r_4] \end{bmatrix} \begin{bmatrix} \dot{i}_1^{(1)} \\ \dot{i}_2^{(1)} \\ \dot{i}_3^{(1)} \\ \dot{i}_4^{(1)} \end{bmatrix} = \\ -\frac{\mu_0\pi}{p^2} \begin{bmatrix} r_1^2 & r_1^2 & r_1^2 & r_1^2 \\ r_1^2 & r_2^2 & r_2^2 & r_2^2 \\ r_1^2 & r_2^2 & r_3^2 & r_3^2 \\ r_1^2 & r_2^2 & r_3^2 & r_4^2 \end{bmatrix} \begin{bmatrix} \dot{i}_1^{(0)} \\ \dot{i}_2^{(0)} \\ \dot{i}_3^{(0)} \\ \dot{i}_4^{(0)} \end{bmatrix} + \begin{bmatrix} \alpha^{(1)} \\ \alpha^{(1)} \\ \alpha^{(1)} \\ \alpha^{(1)} \end{bmatrix}. \end{aligned} \tag{62}$$

Using $\dot{i}_1^{(0)} = \dot{i}_2^{(0)} = \dot{i}_3^{(0)} = 0$ and $\dot{i}_4^{(0)} = \dot{I}_{tot}$, we get

$$\begin{aligned} \log[R/r_1]\dot{i}_1^{(1)} + \log[R/r_2]\dot{i}_2^{(1)} + \log[R/r_3]\dot{i}_3^{(1)} + \log[R/r_4]\dot{i}_4^{(1)} &= -\frac{2\pi^2}{p^2} r_1^2 \dot{I}_{tot} + \alpha^{(1)} \\ \log[R/r_2]\dot{i}_1^{(1)} + \log[R/r_2]\dot{i}_2^{(1)} + \log[R/r_3]\dot{i}_3^{(1)} + \log[R/r_4]\dot{i}_4^{(1)} &= -\frac{2\pi^2}{p^2} r_2^2 \dot{I}_{tot} + \alpha^{(1)} \\ \log[R/r_3]\dot{i}_1^{(1)} + \log[R/r_3]\dot{i}_2^{(1)} + \log[R/r_3]\dot{i}_3^{(1)} + \log[R/r_4]\dot{i}_4^{(1)} &= -\frac{2\pi^2}{p^2} r_3^2 \dot{I}_{tot} + \alpha^{(1)} \\ \log[R/r_4]\dot{i}_1^{(1)} + \log[R/r_4]\dot{i}_2^{(1)} + \log[R/r_4]\dot{i}_3^{(1)} + \log[R/r_4]\dot{i}_4^{(1)} &= -\frac{2\pi^2}{p^2} r_4^2 \dot{I}_{tot} + \alpha^{(1)} \end{aligned} \tag{63}$$

$\alpha^{(1)}$ can be determined by the last equation and $\sum_{n=1}^{N} \dot{i}_n^{(1)} = 0$, but its value is not important here. Taking the difference between 1st and 2nd, between 2nd and 3rd, between 3rd and 4th equations,

we get

$$\begin{aligned}
\log\frac{r_2}{r_1}(\dot{i}_1^{(1)}) &= \frac{2\pi^2}{p^2}(r_2^2-r_1^2)\dot{I}_{tot},\\
\log\frac{r_3}{r_2}(\dot{i}_1^{(1)}+\dot{i}_2^{(1)}) &= \frac{2\pi^2}{p^2}(r_3^2-r_2^2)\dot{I}_{tot},\\
\log\frac{r_4}{r_3}(\dot{i}_1^{(1)}+\dot{i}_2^{(1)}+\dot{i}_3^{(1)}) &= \frac{2\pi^2}{p^2}(r_4^2-r_3^2)\dot{I}_{tot}.
\end{aligned} \tag{64}$$

These equations give $\dot{i}_1^{(1)}$ and $\dot{i}_2^{(1)}$ and $\dot{i}_3^{(1)}$; $\dot{i}_4^{(1)}$ is determined from $\sum_{n=1}^{N}\dot{i}_n^{(1)}=0$.

For $N\to\infty$, and for an arbitrary $n<N$, we get

$$\log\frac{r_{n+1}}{r_n}\left[\sum_{k=1}^{n}\dot{i}_k^{(1)}\right]=\frac{2\pi^2}{p^2}(r_{n+1}^2-r_n^2)\dot{I}_{tot}. \tag{65}$$

Using $r_{n+1}=r_n+\Delta r$, we have $r_{n+1}^2-r_n^2\sim 2r_n\Delta r$ and $\log\frac{r_{n+1}}{r_n}\sim\frac{\Delta r}{r_n}$. Substituting into the above equation, we get

$$\sum_{k=1}^{n}\dot{i}_k^{(1)}=\frac{4\pi^2}{p^2}r_n^2\dot{I}_{tot}\Rightarrow\sum_{k=1}^{n}i_k^{(1)}=\frac{4\pi^2}{p^2}r_n^2 I_{tot}. \tag{66}$$

We have assumed the initial current is zero to obtain the current distribution. As the left-hand side is the current within r_n, this equation is identical to Eq. (52).

VI. CONCLUSION

Bean's critical-state model has been served as the foundation of determining the current and field distributions inside a type-II superconductor under a time-varying external current or magnetic field. Two characteristic features of the Bean model are (i) the amplitude of the SC current density is either zero or at the critical value J_c, and (ii) the change of current distribution begins at the surface and gradually propagates deeper into the superconductor. In this work, we show that the circuit model including inductances and current-dependent resistances are sufficient to explain the Bean-model behavior. In particular, feature (ii) originates from the specific "layered structure" of inductance matrix; feature (i) requires an additional current-dependent resistance that describes the maximum current (density) a superconductor can sustain. Therefore, one can intuitively understand the Bean-model behavior from the interplay between the inductances and the non-linear resistance identified in the circuit model: the inductances dictate how currents change in time and the non-linear resistance makes sure that the current stays below its critical value. It may be worth emphasizing that the circuit model is classical and macroscopic; although peculiar properties of superconductor require atomic-scale modelings involving quantum mechanics, the property of type-II superconductor relevant to the Bean-model behavior is entirely encoded in the macroscopic current-dependent resistance. We have applied the circuit model to a SC slab, a SC wire composed of straight filaments, and a SC wire composed of twisted filaments, and are able to obtain the current distribution, the hysteresis behavior and the heat generation computed using the Bean model. The technical subtleties of solving partial differential equations and the corresponding numerical steps to overcome them are also pointed out. The complete agreement between the circuit model and the Bean model indicates that the circuit model can be a useful formalism to simulate the charging process of multi-filament superconducting wires.

ACKNOWLEDGEMENT

The author thanks Shoichi Yokoyama, Shun Tonooka, Bingnan Wang, Grigory Kolesov, Dongkeun Park, and Yukikazu Iwasa for very helpful discussions.

REFERENCES

[1]A. A. Abrikosov, "On the magnetic properties of superconductors of the second group," Sov. Phys. JETP **5**, 1174 (1957).
[2]A. A. Abrikosov, "Nobel lecture: Type-ii superconductors and the vortex lattice," Rev. Mod. Phys. **76**, 975–979 (2004).
[3]M. N. Wilson, *Superconducting Magnets* (Oxford Science Publication, 1983).
[4]Y. Iwasa, *Case Studies in Superconducting Magnets (2nd Edition)* (Springer, 2009).
[5]M. S. Livingston and J. Blewett, *Particle Accelerators* (McGraw-Hill, New York, 1969).
[6]S. Humphries, *Principled of Charged Particle Acceleration* (Wiley-Interscience, 1986).
[7]D. McRobbie, *MRI from picture to proton* (Cambridge, UK; New York: Cambridge University Press, 2007).
[8]J. Keeler, *Understanding NMR Spectroscopy: Edition 2* (John Wiley and Sons, 2011).
[9]C. P. Bean, "Magnetization of hard superconductors," Phys. Rev. Lett. **8**, 250–253 (1962).
[10]Interim Summary Report on the Analysis of the 19 September 2008 Incident at the LHC, CERN Document EDMS 973073.
[11]Y. B. Kim, C. F. Hempstead, and A. R. Strnad, "Magnetization and critical supercurrents," Phys. Rev. **129**, 528–535 (1963).
[12]M. A. R. LeBlanc, "Magnetization of hard superconductors," Phys. Rev. Lett. **11**, 250–253 (1963).
[13]M. Tinkham, *Introduction to Superconductivity (2nd Edition)* (McGraw-Hill, Inc., 1996).
[14]C. P. Bean, "Magnetization of high-field superconductors," Rev. Mod. Phys. **36**, 31–39 (1964).
[15]R. Hancox, "Enthalpy stabilized superconducting magnets," IEEE Transactions on Magnetics **4**, 486–488 (1968).
[16]P. S. Swartz and C. P. Bean, "A model for magnetic instabilities in hard superconductors: The adiabatic critical state," Journal of Applied Physics **39**, 4991–4998 (1968).
[17]B. Bordini, E. Barzi, S. Feher, L. Rossi, and A. V. Zlobin, "Self-field effects in magneto-thermal instabilities for nb-sn strands," IEEE Transactions on Applied Superconductivity **18**, 1309–1312 (2008).
[18]B. Bordini and L. Rossi, "Self field instability in high-$j_c$$nb_3$snstrands with high copper residual resistivity ratio," IEEE Transactions on Applied Superconductivity **19**, 2470–2476 (2009).
[19]L. Bottura, M. Breschi, and M. Fabbri, "Analytical solution for the current distribution in multistrand superconducting cables," Journal of Applied Physics **92**, 7571–7580 (2002).
[20]L. Bottura, M. Breschi, and M. Fabbri, "Analytical calculation of current distribution in multistrand superconducting cables," IEEE Transactions on Applied Superconductivity **13**, 1710–1713 (2003).
[21]L. Krempasky and C. Schmidt, "Influence of a longitudinal variation of db/dt on the magnetic field distribution of superconducting accellerator magnets," Applied Physics Letters **66**, 1545–1547 (1995).
[22]A. Akhmetov, L. Bottura, M. Breschi, and P. Ribani, "A theoretical investigation on current imbalance in flat two-layer superconducting cables," Cryogenics **40**, 627 – 635 (2000), 4th Workshop on Computation of Thermal Hydraulic Transients in Superconductors.

[23]B. Turck, "Influence of a transverse conductance on current sharing in a two-layer superconducting cable," Cryogenics **14**, 448 – 454 (1974).
[24]T. Tominaka, "Calculations using the helical filamentary structure for current distributions of a six around one superconducting strand cable and a multifilamentary composite," Journal of Applied Physics **96**, 5069–5080 (2004).
[25]T. Tominaka, "Calculations using the helical filamentary structure for current distributions of twisted superconducting multifilamentary composites," Superconductor Science and Technology **18**, 634 (2005).
[26]J. B. Pendry and A. MacKinnon, "Calculation of photon dispersion relations," Phys. Rev. Lett. **69**, 2772–2775 (1992).
[27]It appears that using alternate mesh points is helpful for numerical stability when two coupled functions are related by that the spatial derivative of one function gives the other. Here **j** and **v** have this relationship. In Ref.[26], it is the electric and magnetic fields that have this relationship.
[28]L. N. Cooper, "Bound electron pairs in a degenerate fermi gas," Phys. Rev. **104**, 1189–1190 (1956).
[29]J. Bardeen, L. N. Cooper, and J. R. Schrieffer, "Theory of superconductivity," Phys. Rev. **108**, 1175–1204 (1957).
[30]L. P. Gorkov, "Microscopic derivation of the ginzburg-landau equations in the theory of superconductivity," Sov. Phys. JETP **9**, 1364 (1959).
[31]P. Anderson, "Theory of dirty superconductors," Journal of Physics and Chemistry of Solids **11**, 26 – 30 (1959).
[32]A. Abrikosov, "The magnetic properties of superconducting alloys," Journal of Physics and Chemistry of Solids **2**, 199 – 208 (1957).
[33]U. Essmann and H. Träuble, "The direct observation of individual flux lines in type ii superconductors," Physics Letters A **24**, 526 – 527 (1967).
[34]P. L. Gammel, D. J. Bishop, G. J. Dolan, J. R. Kwo, C. A. Murray, L. F. Schneemeyer, and J. V. Waszczak, "Observation of hexagonally correlated flux quanta in $yba_2cu_3o_7$," Phys. Rev. Lett. **59**, 2592–2595 (1987).
[35]Y. B. Kim, C. F. Hempstead, and A. R. Strnad, "Flux creep in hard superconductors," Phys. Rev. **131**, 2486–2495 (1963).
[36]P. W. Anderson, "Theory of flux creep in hard superconductors," Phys. Rev. Lett. **9**, 309–311 (1962).
[37]J. Bardeen and M. J. Stephen, "Theory of the motion of vortices in superconductors," Phys. Rev. **140**, A1197–A1207 (1965).
[38]M. Tinkham, "Viscous flow of flux in type-ii superconductors," Phys. Rev. Lett. **13**, 804–807 (1964).
[39]J. R. Clem, "Local temperature-gradient contribution to flux-flow viscosity in superconductors," Phys. Rev. Lett. **20**, 735–738 (1968).
[40]B. Maddock, G. James, and W. Norris, "Superconductive composites: Heat transfer and steady state stabilization," Cryogenics **9**, 261 – 273 (1969).
[41]L. Krempasky and C. Schmidt, "Theory of "supercurrents" and their influence on field quality and stability of superconducting magnets," Journal of Applied Physics **78**, 5800–5810 (1995).
[42]Typically, this is done by approximating the mixture of superconductor/normal-conductor by superconductor with a reduced critical current.
[43]J. Duchateau and B. Turck, "Self-field degradation effect in adiabatic conditions," Cryogenics **14**, 481 – 486 (1974).